Available online at www.sciencedirect.com
SCIENCE DIRECT®
Journal of Hydrology 276 (2003) 128–136
Journal of Hydrology
www.elsevier.com/locate/jhydrol

Microscale structural aspects of vegetation density variability

Michael H. Cosh[a,*], Wilfried Brutsaert[a,b]

[a]USDA-ARS, Hydrology and Remote Sensing Lab, Rm 104 Building 007, Beltsville, MD 20705, USA
[b]School of Civil and Environmental Engineering, Hollister Hall, Cornell University, Ithaca, NY 14853, USA

Received 27 February 2002; accepted 24 January 2003

Abstract

Current radiometric remote sensing technology enables high resolution data of vegetation biomass to be obtained in the form of the Normalized Difference Vegetation Index (NDVI). The present study uses such data to examine the spatial structure of vegetation density at the land surface by wavelet, semivariogram, and spectral analyses. Within the range of 30–800 m, the results show that vegetation density of arable cropland is persistent and can be characterized as a fractal with a dimension of 1.59. Within the same range of distances, vegetation density across a more diverse landscape (including besides cropland, also pasture and savanna) exhibits a fractal dimension of 1.69. In the Southern Great Plains, this range is of the order of the typical size of agricultural fields.
© 2003 Elsevier Science B.V. All rights reserved.

Keywords: Vegetation; Fractal dimension; Spectral analysis; Variogram; Variability

1. Introduction

Vegetation density is a valuable land surface parameter for the estimation of land surface-atmosphere interactions. It affects the soil moisture, surface temperature, and the surface energy and water budgets. The spatial variability of vegetation density influences the lower atmospheric circulation and hydrologic processes over a wide range of scales (e.g. Avissar and Pielke, 1989; Li and Avissar, 1994). In the research community, there is a growing awareness of the need to study the variability of vegetation density at scales which cannot be represented efficiently in atmospheric and land surface models (e.g. Atkinson and Tate, 2000). Research has begun to investigate the smaller scale variability of geophysical parameters, such as vegetation density and soil moisture (e.g. Chen and Brutsaert, 1998; Jedlovec and Atkinson, 1992) and how these parameters resemble fractals (e.g. Lam and Quattrochi, 1992; De Jong and Burrough, 1995; Rodriguez-Iturbe et al., 1995).

This paper focuses on the spatial structure of vegetation density at the atmospheric microscale (2 m–2 km) (defined by Orlanski, 1975) on the basis of a fractal approach. Satellite imagery of a summer vegetation scene was obtained for the Southern Great Plains of the United States. This region is typical and representative of other grassland biomes in the world, many of which have undergone profound changes by human activities. Three different

* Corresponding author.
E-mail address: mcosh@hydrolab.arsusda.gov (M.H. Cosh).

0022-1694/03/$ - see front matter © 2003 Elsevier Science B.V. All rights reserved.
doi:10.1016/S0022-1694(03)00068-4

techniques are used to characterize the spatial structure of vegetation density, namely wavelet variance, semivariance, and spectral analyses. From the results of these analyses, conclusions are drawn about the spatial persistence (positive spatial correlation) and distribution of the vegetation density. In particular, the fractal nature of this distribution is investigated. A fractal (self-affine) can be defined as a variable, $y(x)$ which has the cumulative distribution function

$$F(y) = 1 - P\left(\frac{y(x+k) - y(x)}{k^{2-D}} < x_0\right) \quad (1)$$

where $P(\,)$ denotes the probability of the statement inside the brackets, D is the fractal dimension and k is a separation distance (e.g. Turcotte, 1989). A knowledge of the applicability of the fractal distribution to vegetation density will allow future modeling of said parameter to be simulated more accurately (Lam, 1990). One possible approach to characterizing random variability is on the basis of power law distributions. In other words, to be successful, this requires an accurate determination and understanding of the fractal dimension.

2. Vegetation density and NDVI

The study of vegetation is problematic at the scales available by satellite remote sensing because of the wide variety of plant types; therefore, plant type variation is often ignored and instead a single measure of plant biomass is used. For applications with satellite radiometers, several indices have been developed to quantify the 'greenness' of the land surface, which were determined to be good indicators of plant biomass. This study focuses on the Normalized Difference Vegetation Index (NDVI) (Rouse et al., 1974). Further information regarding NDVI can be found in Schowengerdt(1997). This index is defined by

$$\mathrm{NDVI} = \frac{\rho_{\mathrm{NIR}} - \rho_{\mathrm{VIS}}}{\rho_{\mathrm{NIR}} + \rho_{\mathrm{VIS}}} \quad (2)$$

where ρ_{NIR} is the reflectance within the near infrared range (0.7–1.1 μm) and ρ_{VIS} is the reflectance within the visible range (0.4–0.7 μm). Larger values indicate 'greener' surfaces. Conversely, cities and waterways have small values. The data in this study are dominated by green surfaces and there is little effect of urbanization.

3. The satellite data

The Landsat satellites have been providing spectral measurements of the Earth's surface since 1972. More specifically in 1997, the Thematic Mapper (TM) on Landsat-5 was scanning the Earth over seven spectral bands every sixteen days. Two of these bands are useful for estimates of vegetation density. Bands 3 (0.63–0.69 μm) and 4 (0.76–0.90 μm) of TM retrieve visible and near infrared radiance values which are used to calculate of NDVI (Schowengerdt, 1997). The pixels in the radiance images cover areas of approximately 30 m × 30 m.

This study examined two transects selected from a TM-derived NDVI scene recorded over the Southern Great Plains of the United States on July 25, 1997 as part of the Southern Great Plains Experiment 1997 (Jackson, 1999). Several transects were analyzed, but for brevity, these two are presented. Three scenes from a single satellite track were joined to form one image as described in Jackson et al. 1999. The coordinates for each transect are given in Table 1. Transect A is 4096 pixels long or 123 km and 1 pixel (30 m) wide extending east to west along the northern part of the study region. The dominant land use type is cropland, predominantly wheat stubble. Transect B is 16,384 pixels long or 492 km and runs from north to south in the center of the TM image. The land use type along Transect B is more diverse; it includes cropland, pasture, and savanna. In both transects, there are occasional water bodies and

Table 1
Universal transverse Mercator (Zone 14) coordinates for transect A and B of this study

	Transect A	Transect B
Beginning coordinate	563025 E 4193745 N	629285 E 4253715 N
Ending coordinate	685905 E 4193745 N	629285 E 3762195 N

urban areas, but these comprise an insignificant portion of the signal.

4. Method of analysis

4.1. Wavelet variance analysis

Wavelet variance analysis is a powerful tool for describing the strength of persistence for a large data set (Torrence and Compo, 1998). The analysis begins with the wavelet transform, which is defined as the convolution of a filter, $g[(x' - x)/a]$ for a data series, $f(x')$, where a is the scale parameter. This transform is similar to a windowed Fourier transform, but it has the advantage of resolving localized space and wavelength information even the Fourier transform contains only wavelength information. Mathematically, it is calculated by,

$$W(x,a) = \frac{1}{\sqrt{a}} \int_{-\infty}^{+\infty} g\left(\frac{x' - x}{a}\right) f(x')\mathrm{d}x'. \tag{3}$$

The scale parameter represents the effective width of the filter. It also normalizes the resulting signal so that each transform has the same energy (Percival and Walden, 2000). The wavelet filter must satisfy the requirement that its integral is zero, so that after convolution no energy is gained or lost. A common filter is the second derivative of the Gaussian function, also known as the 'Mexican Hat' function. It is defined as

$$g\left(\frac{x' - x}{a}\right) = \left(\frac{1}{2a\pi}\right)^{1/2} \left(1 - \frac{x' - x}{a}\right)^2 \times \exp\left(-\left(\frac{x' - x}{4a}\right)^2\right), \tag{4}$$

and is shown in Fig. 1. After examining alternatives, the 'Mexican Hat' was selected because it is a convenient choice, which is often used to quantify persistence in geophysical data (Malamud and Turcotte, 1999). The second moment of each wavelet transform can be plotted against a to form the wavelet variance function, $V_w(a)$.

$$V_w(a) = \frac{1}{n-1} \sum_{i=1}^{n} (W(x,a) - \bar{W}(a))^2, \tag{5}$$

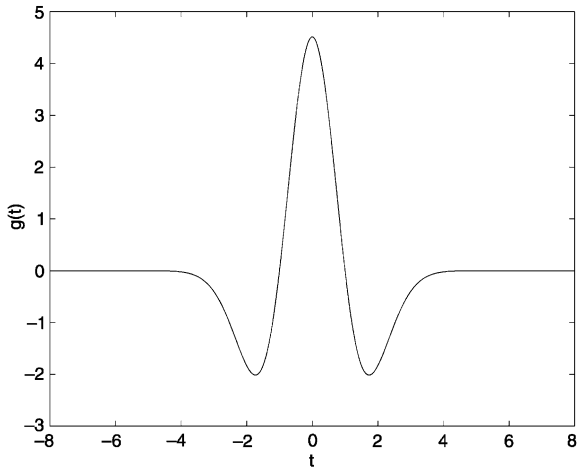

Fig. 1. The Mexican Hat function.

where $\bar{W}(a)$ is the computed average of the wavelet transform for a selected scale parameter, a.

It has also been shown (Malamud and Turcotte, 1999) that if the original data series obeys a power law distribution (and is therefore a fractal), the variance function can be expressed as a power law relation with the form

$$V_w(a) \sim a^{Hw}, \tag{6}$$

where Hw is known as the wavelet exponent.

4.2. Semivariogram analysis

A semivariogram analysis measures the correlation between values in a data series separated by a lag, k (Journel and Huijbregts, 1978; Kitanidis, 1997). The one-dimensional semivariogram is defined as

$$\gamma(k) = \frac{1}{2(N-k)} \sum_{i=1}^{N-k} (Z(X_i) - Z(X_{i+k}))^2 \tag{7}$$

where N is the number of data points in the record and X_i is the ith data point of the distance variable. The semivariogram is often normalized by the variance of the data, so that comparisons can be made between two different functions. While many models can be fitted to the experimental semivariogram, for this study, the power law model was selected, because of its obvious connection with a fractal description. The power law distribution can be written as

$$\gamma(k) \sim k^{2Ha}, \tag{8}$$

where Ha is known as the Hausdorff exponent (Malamud and Turcotte, 1999). Whenever this exponent tends toward zero, the variable can be considered statistically homogeneous (or spatially stationary). This implies that the variable has a constant mean and variance in space; because only these two moments are preserved, this is sometimes also referred to as second order stationarity.

4.3. Spectral analysis

A spectral analysis of a data series reveals its energy distribution for different wavelengths. A discrete Fourier transform decomposes data into a sum of sine and cosine functions. This transform is defined as

$$C_m = \delta \sum_{n=1}^{N} c_n e^{2\pi i n m/N}, \tag{9}$$

where c_n is a discrete data series, N is the length of the series, δ is the distance between data points, and m is an index for the Fourier coefficients (Priestley, 1981). These coefficients are complex numbers of the form $Y_m = a_m + ib_m$, where a_m and b_m are the real and imaginary parts, respectively. The complex modulus of C_m is defined as

$$|C_m| = \sqrt{(a_m^2 + b_m^2)}, \tag{10}$$

which can be used to calculate the power spectral density function. This function is defined as the energy distribution of a signal as a function of wavelength. It is calculated by

$$S(k) = \lim_{N\to\infty} \left(\frac{2|C_m|^2}{N\delta} \right), \tag{11}$$

where $m = 1, 2, 3, \ldots, N/2$, and k is the spatial wavelength (Priestley, 1981). The power spectral density function of a variable with a fractal distribution follows the relation

$$S_k \sim k^{-\beta}, \tag{12}$$

where β is the power spectral density exponent. This exponent can be related to the other exponents mentioned above by the following equation

$$\beta = 2Ha + 1 = Hw = 5 - 2D, \tag{13}$$

where D is the fractal dimension (Malamud and Turcotte, 1999).

Wavelength regression of the power spectral density function to determine a trend line is problematic because of the logarithmic nature of the plot. The shorter wavelengths have more data points, giving that region of the density function more weight in the regression. Therefore, it is useful to divide the function into bins of equal logarithmic size so that no region dominates the regression. The loss of spectral information to neighboring wavelengths, known as leakage, can be a problem with discrete Fourier transforms. This problem can be alleviated by using a window function on the data (Percival and Walden, 1993). The Welch window is commonly used for this and is defined as

$$w_n = 1 - \left(\frac{n - (N/2)}{N/2} \right)^2, \tag{14}$$

where $n = 1, 2, \ldots, N$. In practice, the data series is multiplied by this window function before the spectral analysis is carried out (Malamud and Turcotte, 1999).

5. Analysis and results

5.1. Transect A

The first step in this work was to compute the wavelet transforms of the data set. A Mexican Hat function was convolved with Transect A to generate wavelets for eight levels of analysis. The initial window had a width of 16 data points (8 on each side) and is referred to as $a = 1$. This window length was doubled for each successive scale, namely to 32 data points ($a = 2$), 64($a = 4$), etc. The resulting wavelet scales of analysis are shown in Fig. 2 together with the original signal. It is observed in the original signal that there are several downward spikes which represent water bodies on the scale of less than 1 km.

The variance was calculated for each wavelet scale and plotted as a logarithm against the scale parameter a in Fig. 3. Power law regressions for the spectral density functions of vegetation density (Eq. (4)) were calculated for $a =$ 1–8. The regression equation (Eq. (6)) for the resulting variances gives the function

$$V_w(a) = 0.0472a^{1.829}, \tag{15}$$

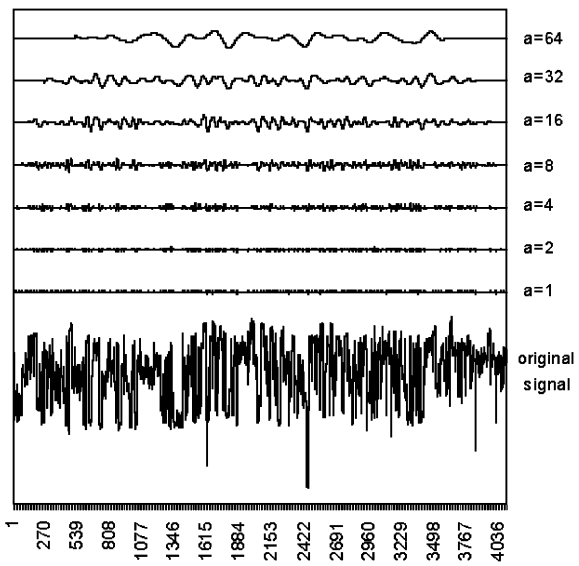

Fig. 2. Results of wavelet variance analysis for Transect A. The original series is indicated at the bottom and the wavelet transforms are plotted in ascending order. The *x*-axis is measured in pixels and the *y*-axis is scaled to fit on one plot. The relative magnitudes of each signal have been maintained.

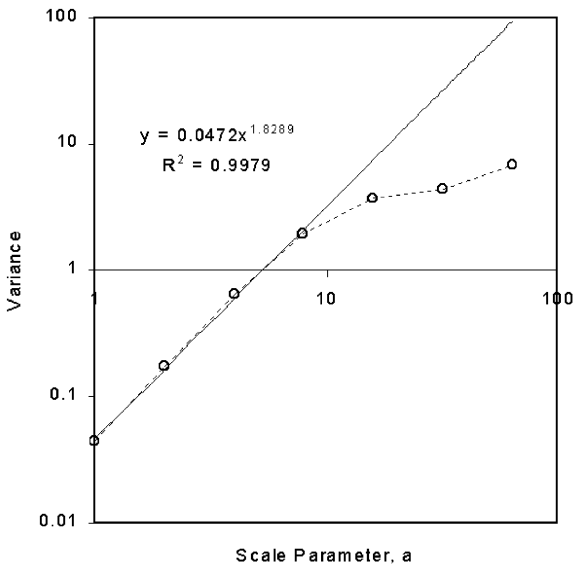

Fig. 3. Wavelet variance function for the wavelet transforms for Transect A. The R^2 and regression equation is for the first four points of the signal. The function was scaled by the variance of the entire signal.

where 1.829 is the value of *Hw*. The variance function of the wavelets started to deviate from the power law beyond $a = 8$ (point 4), which is equivalent to 960 m. This is roughly the length of the average agricultural field, also referred to as a quarter-section. For the first four points, the regression has an R^2 of 0.998, indicating a very strong relationship between the data and the regression equation.

The semivariogram of Transect A is shown in Fig. 4. This confirms that the choice of a power law relationship (Eq. (8)) is indeed appropriate for the initial 400 m; the corresponding regression equation is

$$\gamma_k = 0.00450k^{0.826}, \tag{16}$$

with a value of *Ha* equal to 0.413 for the range of 30–400 m. This distance is approximately half the length of the average agricultural field. This analysis depends on pairs of points which are separated by a lag. When that lag reaches half the length of a field, approximately half of the pairs include points in different fields, which may have different crops. Therefore it is not surprising that instead of a breakpoint at 800 m, the semivariogram breaks at 400 m. The semivariogram reaches an upper bound at about 2 km, which indicates

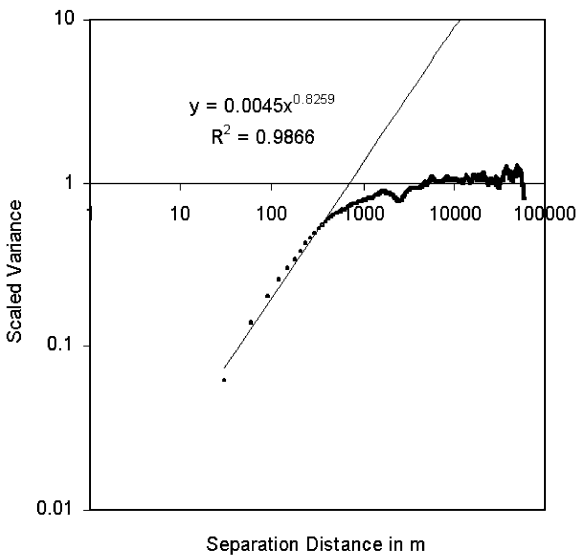

Fig. 4. Semivariogram for Transect A with a regression trend line calculated for the region of 30 m–400 m.

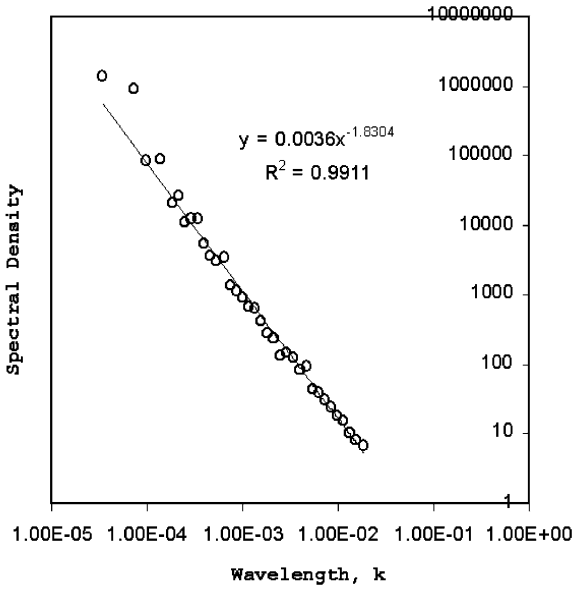

Fig. 5. Power spectral density function for Transect A. The function is averaged of logarithmic bins of equal size. A regression line is also plotted with it's descriptive equation.

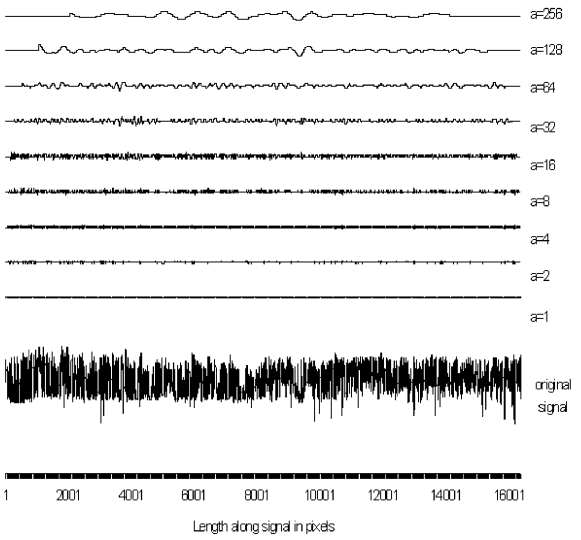

Fig. 6. Results of wavelet variance analysis for Transect B. The original series is indicated at the bottom and the wavelet transforms are plotted in ascending order. The *x*-axis is measured in pixels and the *y*-axis is scaled to fit on one plot. The relative magnitudes of each transform have been maintained.

a second order stationary process at scales larger than that.

For the spectral analysis, Transect A was divided into four smaller segments, each with a length of 1024 pixels (30 km) to increase the number of sample transects. The resulting power spectral density functions were then averaged to reduce noise. A power law regression (Eq. (12)) was calculated for the averaged signal, and yielded

$$S_k = 0.00360k^{-1.830}, \tag{17}$$

with a β value of 1.830. The power spectral density function is shown in Fig. 5 with logaritmic bins. A break point is observed in the function at a wavelength of approximately 400 m for the same reason as explained for Fig. 3.

To repeat briefly, the three analyses produced $Hw = 1.829$, $Ha = 0.413$, and $\beta = 1.830$, resulting in fractal dimension, D, estimates of 1.586, 1.587, and 1.585 respectively, calculated from (Eq. (13)). An average fractal dimension can be calculated to be 1.586. This indicates that for the range of 30 m–800 km, the data appear to obey a power relationship fairly well.

5.2. Transect B

This transect was analyzed in the same manner as Transect A. A plot of each wavelet transform and the original signal is shown in Fig. 6. The wavelet variance analysis of Transect B is shown in Fig. 7. The power law relation (Eq. (6)) for the first four points was calculated as

$$V_w(a) = 0.0457a^{1.6256}, \tag{18}$$

with a β of 1.626. This relationship applies to the range of 30–960 m, as was the case for Transect A. Beyond 960 m, the variances do not appear to follow the power law relationship. The R^2 for the regression of the first four points is 0.996, again indicating a very strong correspondence between the data and Eq. (18).

The semivariogram analysis of Transect B was fitted by a power law function (Eq. (8)), and this produced

$$\gamma_k = 0.0182k^{0.619}, \tag{19}$$

with a value of Ha equal to 0.309 for wavelengths up to 400 m. The details are shown in Fig. 8. The

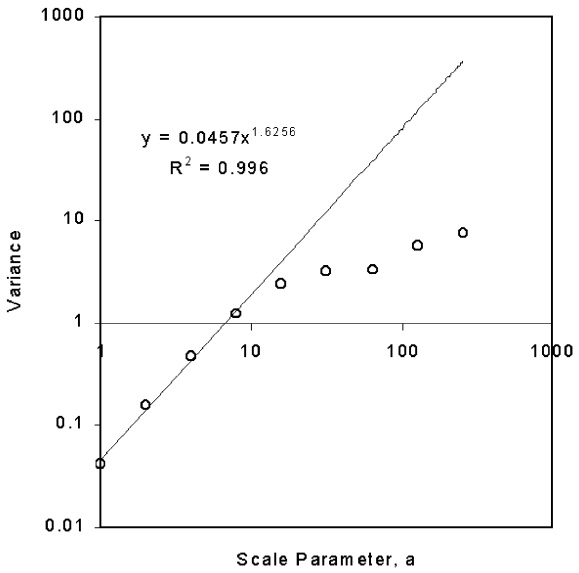

Fig. 7. Wavelet variance function for Transect B. The R^2 and regression equation are for the first four points of the signal. The function was scaled by the variance of the entire signal.

semivariogram reaches its sill at 1 km, the range of spatial autocorrelation.

For the spectral analysis of Transect B, the data were divided into 4 smaller segments each with a length of 4096 pixels or 120 km. Again, the resulting

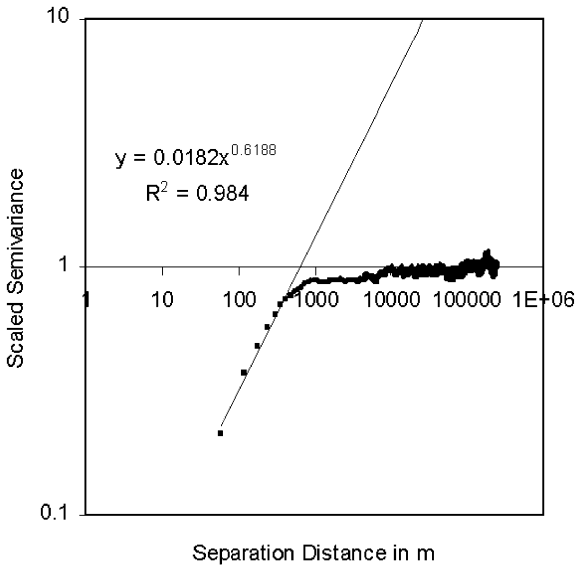

Fig. 8. Semivariogram for Transect B with a regression trend line calculated for the region of 30–400 m.

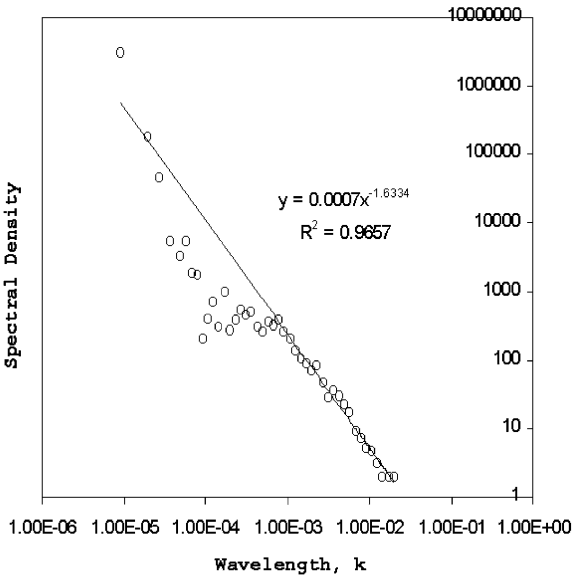

Fig. 9. Power spectral density function for Transect B. The function is averaged with logarithmic bins of equal size. A regression line is also plotted with it's descriptive equation.

power spectral density functions were averaged to reduce noise. The analysis revealed a power law relation (Eq. (12)), namely

$$S_k = 0.00250k^{-1.660}, \tag{20}$$

giving a β value of 1.660 for the range of 30 m–1.0 km. The logarithmically binned power spectral density function is plotted in Fig. 9.

These three analyses produced the following results: $Hw = 1.626$, $Ha = 0.309$, and $\beta = 1.6334$. The estimates of the fractal dimension, D, were calculated from (Eq. (13)), namely 1.687, 1.691, and 1.683, and averaged to produce a mean fractal dimension for Transect B of 1.687.

6. Conclusions

The power law distribution of vegetation density was established by each of the three methods of analyses. Table 2 contains a summary of the results of these analyses. Wavelet variance analysis demonstrates a strong persistence and a power law relationship for the first four data points in both transects, covering approximately 960 m. This length

Table 2
A summary of the exponents from each analysis for both transects and the estimated *D*s for both transects. Arithmetic averages are calculated from the estimates of *D*

	Coefficient	Estimate	Estimated *D*
Transect A	Hw	1.829	1.586
	Ha	0.413	1.587
	β	1.830	1.585
	Average	1.586	
Transect B	Hw	1.626	1.687
	Ha	0.309	1.691
	β	1.633	1.683
	Average	1.687	

is of the order of the average length of large agricultural fields in the Southern Great Plains, which are approximately 800 m. Much of the land is this region was divided into square mile sections and these sections were then divided into at least four fields with a length of one half mile or 800 m. From visual inspection of the NDVI image, it was observed that the typical road spacing was 1 mile and each block was divided into four sections. Semivariogram analysis confirmed the power law distribution; however, only up to a scale of half of the average agricultural field, or 400 m. This anomaly may be attributed to a natural bias of semivariograms for data with heterogeneity such as NDVI for cropland. Indeed, for distances larger than half of the field size, a larger number of pairs of points used to calculate the semivariogram will be sampled from adjacent agricultural fields with a different crop. The spectral density function also corroborated the power law exponent. The estimated fractal dimension of this distribution is 1.586 for cropland. For a more diverse landscape, containing cropland, pasture, and savanna, the fractal dimension was estimated to be 1.687. These dimensions indicate a signal with strong long-range persistence and the signal can be referred to as a fractional motion (Malamud and Turcotte, 1999). A fractal dimension for a Brownian motion is 1.5 for comparison. Therefore, the NDVI values observed in this study are more persistent than a Brownian motion. At distances greater than 1 km, the semivariogram analysis indicates that NDVI reaches an upper bound. This will have significant implications for the parameterization of vegetation density in land surface modelling, because the variability can be assumed to be constant (or stationary) beyond that scale. Furthermore, the persistence of the data at scales smaller than 800 m makes dense data sampling unnecessary. Clearly, it has implications on the modelling of its spatial variability at these smaller scales as well. In any type of modelling of the variability in a non-deterministic way, knowledge of the fractal dimension is required.

The variability of vegetation density appears to have a similar structure to that of surface soil moisture analyzed in other studies. Pelletier et al. (1997) determined that soil moisture fields follow a power law distribution with a β value of 1.8 at scales smaller than 2 km and Rodriguez-Iturbe et al. (1995) established that the scale invariance continued down to a scale of 30 m. The present study established that the exponent of the spectral density function is $\beta = 1.830$ for cropland. This strongly suggests that there is a proportional relationship between the scale invariance, that is the fractal nature, of the density of uniform vegetation (consisting of the same crop species) and that of surface soil moisture at scales smaller than 800 m.

Acknowledgements

The authors would like to thank Donald Turcotte for his generous contributions to this article. This research was conducted with the cooperation of the US Department of Energy as part of the Atmospheric Radiation Measurement Program. In addition, this work has been supported by grants ATM-9708622 from the National Science Foundation and NAG8-1518 from the National Aeronautics and Space Administration

References

Atkinson, P.M., Tate, N.J., 2000. Spatial scale problems and geostatistical solutions: a review. Professional Geographer 52, 607–623.

Avissar, R., Pielke, R.A., 1989. A parameterization of heterogeneous land surfaces for atmospheric numerical models and its impact on regional meteorology. Mon. Wea. Rev. 117, 2113–2136.

Chen, D., Brutsaert, W., 1998. Satellite-sensed distribution and spatial patterns of vegetation parameters over a tallgrass prairie. J. Atmos. Sci. 55, 1225–1238.

De Jong, S.M., Burrough, P.A., 1995. A fractal approach to the classification of Mediterranean vegetation types in remotely sensedimages. Photogrammetric Engng Remote Sensing 61 (8), 1041–1053.

Jackson, T.J., 1999. Remote Sensing of Soil Moisture in the Southern Great Plains Hydrology Experiment, International Geoscience and Remote Sensing Symposium (IGARSS) 2, Jun 28–Jul 2, IEEE, pp. 1158–1160.

Jackson, T.J., Le Vine, D.M., Hsu, A.Y., Oldak, A., Starks, P.J., Swift, C.T., Isham, J.D., Haken, M., 1999. Soil moisture mapping at regional scales using microwave radiometry: the Southern Great Plains hydrology experiment. IEEE Trans. Geosc. Rem. Sens. 37 (5), 2136–2151.

Jedlovec, G.J., Atkinson, R.J., 1992. Variability of geophysical parameters from aircraft radiance measurements for FIFE. J. Geophys. Res., 97 D17, 18,913–18,924.

Journel, A.G., Huijbregts, C.J., 1978. Mining Geostatistics, Academic Press, London.

Kitanidis, P.K., 1997. Introduction to Geostatistics, Cambridge University Press, New York.

Lam, N.S.-N., 1990. Description and measurement of Landsat TM images using fractals. Photogrammetric Engng Remote Sensing 56 (2), 187–195.

Lam, N.S.-N., Quattrochi, D.A., 1992. On the issues of scale, resolution, fractal analysis in the mapping sciences. Professional Geographer 44, 88–98.

Li, B., Avissar, R., 1994. The impact of spatial variability of land-surface characteristics on land-surface heat fluxes. J. Climate 7, 527–537.

Malamud, B.D., Turcotte, D.L., 1999. Self-affine time series: I. Generation and analyses. Adv. Geophys. 40, 1–90.

Orlanski, I., 1975. A rational subdivision of scales for atmospheric processes. Bull. Am. Met. Soc. 56, 527–530.

Pelletier, J.D., Malamud, B.D., Blodgett, T., Turcotte, D.L., 1997. Scale-invariance of soil moisture variability and its implications for the frequency-size distribution of landslides. Engng Geol. 48, 255–268.

Percival, D.B., Walden, A.T., 1993. Spectral Analysis for Physical Applications: Multitaper and Conventional Univariate Techniques, Cambridge University Press, Cambridge.

Percival, D.B., Walden, A.T., 2000. Wavelet Methods for Time Series Analysis, Cambridge University Press, London.

Priestley, M., 1981. Spectral Analysis and Time Series, Academic Press, New York.

Rodriguez-Iturbe, I., Vogel, G.K., Rigon, R., Entekhabi, D., Castelli, F., Rinaldo, A., 1995. On the spatial organization of soil moisture fields. Geophys. Res. Lett. 22 (20), 2757–2760.

Rouse, J.W., Haas, R.H., Deering, D.W., Schell, J.A. Monitoring the vernal advancement and retrogradation (Green wave effect) of natural vegetation. Final Rep. RSC 1978-4, Remote Sensing Center, Texas A&M Univ., College Station, 1974.

Schowengerdt, R.A., 1997. Remote Sensing: Models and Methods for Image Processing, Academic Press, San Diego, CA.

Torrence, C., Compo, G.P., 1998. A practical guide to wavelet analysis. Bull. Am. Met. Soc. 79 (1), 61–78.

Turcotte, D.L., 1989. Fractals and Chaos in Geology and Geophysics, Cambridge University Press, UK, p. 221.